CRYSTAL GROWTH & DESIGN

Article

pubs.acs.org/crystal

High Brightness and Easy Color Modulation in Lanthanide-Based Coordination Polymers with 5-Methoxyisophthalate as Ligand: Toward Emission Colors Additive Strategy

Insa Badiane,[†,‡] Stéphane Freslon,[†] Yan Suffren,[†] Carole Daiguebonne,*[,†] Guillaume Calvez,[†] Kevin Bernot,[†] Magatte Camara,[‡] and Olivier Guillou*[,†]

[†]UMR 6226 "Institut des Sciences Chimiques de Rennes", INSA Rennes, 20 Avenue des buttes de Coësmes, F35708 Rennes, France

[‡]LCPM−Groupe "Matériaux Inorganiques: Chimie Douce et Crystallographie", Université Assane Seck de Ziguinchor, BP 523 Ziguinchor, Sénégal

Supporting Information

ABSTRACT: Reactions in water between lanthanide chlorides and the disodium salt of 5-methoxyisophthalic acid, $Na_2(mip)\cdot 7H_2O$, lead to the first three series of lanthanide-based coordination polymers based on this ligand. The first series contains only one compound with chemical formula $[Ce(mip)_{3/2}(H_2O)_5\cdot 2H_2O]_\infty$. The second series has general chemical formula $[Ln(mip)\ (Hmip)(H_2O)_5\cdot H_2O]_\infty$ with Ln = La−Ce. The last family is constituted by compounds with general chemical formula $[Ln_2(mip)_3(H_2O)_8\cdot 4H_2O]_\infty$ with Ln = Sm−Er plus Y. Luminescent properties of the compounds that belong to this family have been studied. The Tb-based compound presents one of the brightest luminescences reported to date for a lanthanide-based coordination polymer. The weak intermetallic energy transfer evidenced on the third family of compounds allows easy and predictable color modulation of the heterobimetallic powders through additive colors strategy.

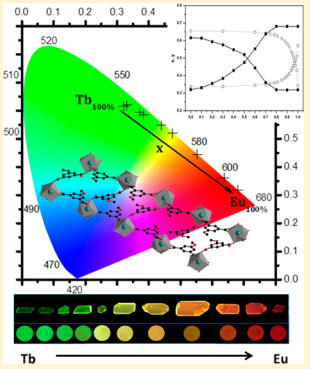

INTRODUCTION

Lanthanide-based coordination polymers have attracted great interest in the past 2 decades because of their potentially interesting porosity,[1−9] magnetic,[10−13] or optical[14−22] properties for example. More recently, lanthanide-based coordination polymers have proved their interest as taggants for the fight against counterfeiting[23] because they can present highly flexible luminescence.[24,25] Some of us have been engaged in the synthesis and study of lanthanide-based coordination polymers for more than 20 years,[26] mainly focusing attention on benzene−polycarboxylate ligands.[27] In recent years we have studied several series with isophthalate derivatives as ligands[28−32] (see Scheme 1).

These series that present almost isoreticular crystal structures (Figure 1) exhibit promising optical properties that arise from competing transfers (ligand-to-metal and metal-to-metal energy transfers, photoinduced electron transfer, and so on). These promising optical properties have encouraged us to undertake the study of lanthanide-based coordination polymers with 5-methoxyisophthalate ligand hereafter referred to as $(mip)^{2-}$.

To the best of our knowledge, some coordination polymers based on $(mip)^{2-}$ ligand and involving transition metal ions have recently been reported[33−35] but, to date, none of them involves lanthanide ions. We want to report here the first three series of lanthanide-containing coordination polymers based on this ligand.

EXPERIMENTAL SECTION

Synthesis and Characterization of the Ligand. 5-Methoxyisophthalic acid has been purchased from TCI (98%) and used without further purification. A 2 equiv amount of sodium hydroxide is added to an aqueous suspension of 5-methoxyisophthalic acid. The obtained clear solution is then evaporated to dryness, and the residual solid is dissolved in ethanol and refluxed for 1 h. Then precipitation is provoked by addition of an excess of ethoxyethane. The white precipitate is filtered and washed with ethoxyethane. After recrystallization in deionized water, the powder is filtered and dried under ambient conditions. The yield is about 90%. Recrystallization has provided single crystals suitable for X-ray structure determination (Figure 2). Selected crystal and final structure refinement data are listed in Table 1.

Powder X-ray diffraction patterns indicate that the powder and the single crystal are isostructural (Supporting Information Figure S1). Chemical analysis for $Na_2C_9H_{20}O_{12}$ (MW = 366 g mol^{-1}) found (calcd): Na, 12.4% (12.5%); C, 29.4% (29.5%); H, 5.6% (5.5%); O, 52.6% (52.5%).

The IR spectrum does not show any characteristic band of protonated carboxylate functions (1410 cm^{-1}). Thermal analyses confirm the departure of seven water molecules (exptl, 34.0%; calcd, 34.4%). First, there is a first weight loss between 50 and 150 °C that corresponds to six water molecules (exptl, 29.3%; calcd, 29.5%). The seventh one is removed between 150 and 200 °C (exptl, 4.7%; calcd, 4.9%). This assumption is supported by IR spectra of the exhausted

Received: November 4, 2016
Revised: February 7, 2017
Published: February 7, 2017

DOI: 10.1021/acs.cgd.6b01607
Cryst. Growth Des. 2017, 17, 1224−1234

Scheme 1. Schematic Representation of Ligands Investigated by Our Group: Isophthalic Acid (H_2ip),[32] 5-Aminoisophthalic Acid (H_2aip),[28,31] 5-Hydroxyisophthalic acid (H_2oip),[30] and 5-Methoxyisophthalic Acid (H_2mip; This Work) (Left to Right)

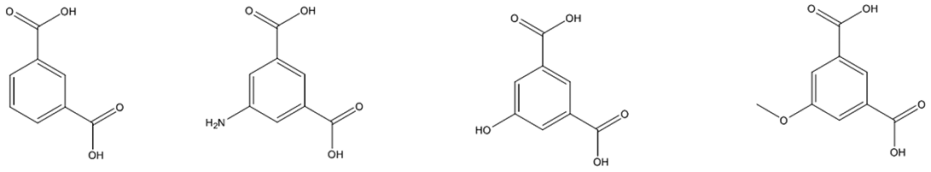

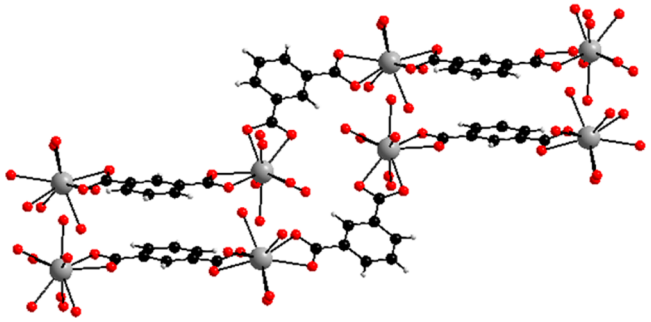

Figure 1. Projection view of a zigzag double-chains molecular motif of $[Gd_2(ip)_3(H_2O)_9{\cdot}6H_2O]_\infty$. Drawn from data in ref 32. This molecular motif is also encountered in crystal structures of 5-aminoisophthalate- and 5-hydroxyisophthalate-based lanthanide coordination polymers.[28,30,31]

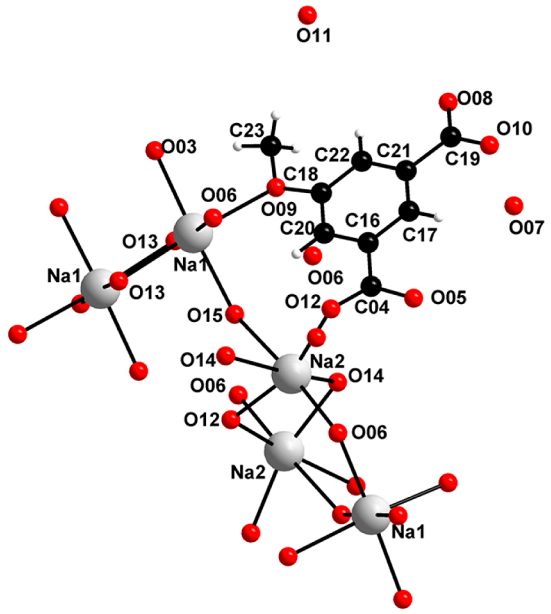

Figure 2. Projection view of an extended asymmetric unit of Na_2(mip)·$7H_2O$.

gas that have been recorded all along the thermal analysis (Figure S2). The liquid UV−visible absorption spectrum of a diluted aqueous solution (2.73×10^{-4} mol L^{-1}) of Na_2(mip)·$7H_2O$ presents a maximum at 299 nm with ε_{299} = 4320 L mol^{-1} cm^{-1} (Figure S3).

Synthesis and Characterization of the Coordination Polymers as Single Crystals. Lanthanide oxides (99.99%) were purchased from the AMPERE Co. The chlorides were prepared according to literature procedures.[36] Tetramethylorthosilicate (TMOS) and agarose gels were purchased from Acros Organics and used without further purification. They were jellified according to established procedures.[37−39] Dilute aqueous solutions (0.1 mol L^{-1}) of the lanthanide chloride on one hand and of the disodium salt of methoxyisophtalate on the other hand were allowed to slowly diffuse

Table 1. Crystal and Final Structure Refinement Data for Na_2(mip)·$7H_2O$

mol formula	$Na_2O_{12}C_9H_{20}$
syst	monoclinic
a (Å)	12.4922(6)
b (Å)	7.1710(3)
c (Å)	17.6871(8)
β (deg)	96.114(2)
V (Å^3)	1575.43(12)
Z	4
FW (g mol^{-1})	366.12
space group (No.)	$P2_1/n$ (14)
D_{calc} (g cm^{-3})	1.485
μ (mm^{-1})	0.185
R (%)	6.20
R_W (%)	22.20
GoF	0.999
CCDC no.	1501139

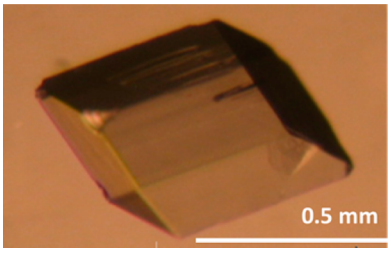

Figure 3. Picture of a single crystal of $[La(mip)\ (Hmip)(H_2O)_5{\cdot}H_2O]_\infty$.

through a gel bridge in U-shaped tubes. After a few weeks, single crystals suitable for X-ray structure determination were obtained (see Figure 3 for an example).

Three types of crystal structures were identified depending on the involved lanthanide ion. Results are summarized in Table 2.

Synthesis and Characterization of the Coordination Polymers as Microcrystalline Powders. Microcrystalline powders of the coordination polymers were obtained by mixing stoichiometric aqueous solutions of a lanthanide chloride (1 mmol in 20 mL of deionized water) and of disodium methoxyisophthalate (1.5 mmol in 20 mL of deionized water). Precipitations immediately occurred. Microcrystalline powders were filtered and dried in air. Yields were close to 90%. Chemical analyses of the microcrystalline powders have been listed in Table S1. On the basis of their powder X-ray diffraction diagrams, microcrystalline powders were classified in two series (see Figures S4 and S5): The first series contains the compounds that have been obtained with lanthanum or cerium while the second one contains compounds obtained with one of the lanthanide ions comprised between samarium and ytterbium plus yttrium. Other lanthanide ions lead to amorphous powders. Compounds that belong to the first family are isomorphous to $[Gd(mip)\ (Hmip)(H_2O)_5{\cdot}H_2O]_\infty$, and those that belong to the second family are isomorphous to $[Y_2(mip)_3(H_2O)_8{\cdot}4H_2O]_\infty$. Both crystal structures are described hereafter. It can be noticed that no microcrystalline powder presents a

DOI: 10.1021/acs.cgd.6b01607
Cryst. Growth Des. 2017, 17, 1224−1234

Table 2. Structural Classification of the Microcrystalline Powders and of the Single Crystals

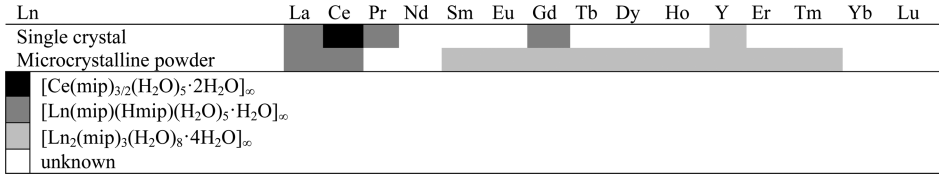

Table 3. Crystal and Final Structure Refinement Data for $[Ce(mip)_{3/2}(H_2O)_5{\cdot}2H_2O]_\infty$, $[Gd(mip)\ (Hmip)(H_2O)_5{\cdot}H_2O]_\infty$, and $[Y_2(mip)_3(H_2O)_8{\cdot}4H_2O]_\infty$

mol formula	$Ce_2C_{27}H_{46}O_{29}$	$GdO_{16}C_{18}H_{25}$	$Y_2O_{27}C_{27}H_{18}$
syst	monoclinic	triclinic	monoclinic
a (Å)	10.8750(2)	7.4437(3)	17.4214(11)
b (Å)	10.6070(1)	10.9493(4)	10.7884(8)
c (Å)	18.4790(2)	14.5247(6)	20.3688(15)
γ (deg)		89.238(2)	
β (deg)	100.700(1)	83.423(2)	104.136(2)
γ (deg)		78.619(2)	
V (Å^3)	2094.51(1)	1152.84(8)	3712.4(5)
Z	2	2	4
FW (g mol^{-1})	1114.88	654.53	952.23
space group (No.)	$P2_1/c$(14)	$P\bar{1}$ (2)	$P2_1/n$ (14)
D_{calc} (g cm^{-3})	1.768	1.851	1.704
μ (mm^{-1})	2.242	2.955	3.211
R (%)	5.14	2.86	3.33
R_W (%)	16.30	8.16	10.19
GoF	1.083	1.101	1.055
CCDC no.	1505544	1501131	1501130

powder X-ray diffraction diagram that corresponds to $[Ce(mip)_{3/2}(H_2O)_5{\cdot}2H_2O]_\infty$ (Table2).

Single-Crystal X-ray Diffraction. Single crystals of $Na_2(mip){\cdot}7H_2O$ and of $[Gd(mip)\ (Hmip)](H_2O)_5{\cdot}H_2O]_\infty$ were mounted on a APEXII AXS-Bruker diffractometer (150 K) with Mo Kα radiation (λ = 0.71073 Å) and a single crystal of $[Y_2(mip)_3(H_2O)_8{\cdot}4H_2O]_\infty$ and $[Ce(mip)_{3/2}(H_2O)_5{\cdot}2H_2O]_\infty$ on a D8Venture Bruker AXS diffractometer with multilayers monochromatized Mo Kα radiation and equipped with a CMOS PHOTON100 detector (300 K). Data reduction and cell refinement were performed with Denzo and Scalepack programs[40] or Apex3(2015), Saint(V8.37a) and Sadabs-(2014/5)[41−43] according to the used diffractometer. The crystal structures have been solved by direct methods using the SIR97 program,[44] and refined with full matrix least-squares methods based on F^2 (SHELX97[45]) with WINGX program.[46] All non-hydrogen atoms were refined anisotropically using the SHELXL program. Hydrogen atoms bound to the organic ligand were located at ideal positions except those bound to the disordered ligand in the crystal structure of $[Ce(mip)_{3/2}(H_2O)_5{\cdot}2H_2O]_\infty$ that have not been located. Hydrogen atoms of the water molecules were not located. Crystal and final structure refinement data of $Na_2(mip){\cdot}7H_2O$ are listed in Table 1 and those of $[Ce(mip)_{3/2}(H_2O)_5{\cdot}2H_2O]_\infty$, $[Gd(mip)\ (Hmip)](H_2O)_5{\cdot}H_2O]_\infty$, and of $[Y_2(mip)_3(H_2O)_8{\cdot}4H_2O]_\infty$ in Table 3. Full details of the X-ray structure determination of the four crystal structures have been deposited with the Cambridge Crystallographic Data Center under the depository numbers CCDC 1501139 ($Na_2(mip){\cdot}7H_2O$), CCDC 1505544 ($[Ce(mip)_{3/2}(H_2O)_5{\cdot}2H_2O]_\infty$), CCDC 1501131 ($[Gd(mip)(H(mip)(H_2O)_5{\cdot}H_2O]_\infty$), and CCDC 1501130 ($[Y_2(mip)_3(H_2O)_8{\cdot}4H_2O]_\infty$). They can be obtained free of charge at http://www.ccdc.cam.ac.uk/conts/retrieving.html or, on request, from the authors with reference to this publication.

Powder X-ray Diffraction. The diagrams have been collected using a PanalyticalX'Pert Pro diffractometer equipped with an X'Celerator detector. Calculated patterns were produced using POWDERCELL and WINPLOTR software programs.[47,48]

Thermal dependent X-ray diffraction diagrams have been produced with the same diffractometer. The samples were heated from room temperature to 1000 °C using an Anton Parr HTK 1200 furnace under nitrogen atmosphere.

Solid State Luminescent Measurements. Solid state emission and excitation spectra have been measured on a Horiba Jobin-Yvon Fluorolog III fluorescence spectrometer equipped with a 450 W Xe lamp and a UV−vis photomultiplier (Hamamatsu R928; sensitivity, 190−860 nm). Most of the luminescence spectra were recorded between 350 and 725 nm at room temperature. The quantum yield measurements were performed using a Jobin-Yvon integrating sphere ($\Phi = (E_c - E_a)/(L_a - L_c)$ with E_c being the integrated emission spectrum of the sample, E_a the integrated "blank" emission spectrum, L_a the "blank" absorption, and L_c the sample absorption at the excitation wavelength). The emission/excitation spectra and quantum yield recordings were realized on powder samples introduced in cylindrical quartz cells of 0.7 cm diameter and 2.4 cm height, which were placed directly inside the integrating sphere. The luminescence of the Gd-based microcrystalline powder has been measured at 77 K; the sample was introduced in a quartz capillary tube, which was placed inside a small Dewar containing nitrogen liquid. Luminescence decays have also been measured at room temperature using this apparatus with a Xe flash lamp (phosphorescence mode). Lifetimes and quantum yields are averages of three independent determinations. Appropriate filters were used to remove the residual excitation laser light, the Rayleigh scattered light, and associated harmonics from spectra. All spectra were corrected for the instrumental response function.

Comparative solid state luminescent spectra have been measured on a PerkinElmer LS-55 spectrometer with a Xe flash lamp and equipped with a UV−vis photomultiplier (Hamamatsu R928) between 450 and 725 nm under identical operating conditions and without turning the lamp off to ensure a valid comparison between the emission spectra. All spectra have been recorded with the phosphorescence mode, not with the standard fluorescence mode (delay and gate times were applied to remove residual light from the sample holder). Automatic filters were also used during the measurements as for the Fluorolog III.

Luminescence intensities of the samples expressed in cd m^{-2} have been measured with a Gigahertz-Optik X1-1 optometer with an integration time of 200 ms on 1.5 cm^2 pellets. The intensity of the UV flux at the sample location, 0.385 mW cm^{-2}, has been measured with a VilberLourmat VLX-3W radiometer. $[Tb_2(bdc)_3{\cdot}4H_2O]_\infty$, where bdc^{2-} stands for terephthalate, was used as a standard. Its luminance is 142 cd m^{-2} under these operating conditions (λ_{exc} = 312 nm; flux = 0.385 mW cm^{-2}).[49]

Colorimetric Measurements. The CIE (Commission Internationale de l'Eclairage) (x,y) emission color coordinates[50,51] were obtained using a MSU-003 colorimeter (Majantys) with the PhotonProbe 1.6.0 Software (Majantys). Color measurements were taken under the following conditions: 2°, CIE 1931, step 5 nm, under 312 nm UV light. $X = k\int_{380nm}^{780nm} I_\lambda x_\lambda$, $Y = k\int_{380nm}^{780nm} I_\lambda y_\lambda$, and $Z = k\int_{380nm}^{780nm} I_\lambda z_\lambda$ with k being a constant for the measurement system I_λ sample spectrum intensity, wavelength dependent, and x_λ, y_λ, and z_λ being trichromatic values $x = X/(X + Y + Z)$, $y = Y/(X + Y + Z)$, and $z = Z/(X + Y + Z)$. Mean xyz values are given for each sample, which act as light sources (luminescent samples). The following standards from Phosphor Technology were used, calibrated at 312 nm: red phosphor Gd_2O_2S:Eu (x = 0.667; y = 0.330) and green phosphor Gd_2O_2S:Tb (x = 0.328; y = 0.537).

Coupled Thermal and IR Analyses. Coupled thermal (ATG/DSC) and IR analyses have been performed using a PerkinElmer

DOI: 10.1021/acs.cgd.6b01607
Cryst. Growth Des. 2017, 17, 1224−1234

STA6000 thermal analyzer coupled to a PerkinElmer Frontier IR spectrophotometer analyzer. Coupling was ensured by a PerkinElmer TL8000 transfer line. This allows simultaneous recording of the weight of the sample, the heat flux, and the IR spectrum of the exhausted gases versus temperature. Measurements were performed in ceramic crucibles under a nitrogen atmosphere between room temperature and 900 °C with a 20 °C min^{-1} heating rate. At the end of the experiment, the compound was maintained for 1 h at 900 °C under air atmosphere in order to complete the combustion.

RESULTS AND DISCUSSION

$[Ce(mip)_{3/2}(H_2O)_5{\cdot}2H_2O]_\infty$. This compound has been obtained as single crystals only. Its crystal structure can be described as the superimposition of 1D molecular chains in which Ce^{3+} ions and $(mip)^{2-}$ ligands alternate (Figure 4). There is only one independent Ce^{3+} ion in the crystal structure that is nine coordinated by five oxygen atoms from coordination water molecules and four oxygen atoms from two carboxylate clips that form a slightly distorted muffin (Table S2). A fully deprotonated ligand with a half-occupancy factor is located between the chains and ensures the electroneutrality of the crystal packing. Stability of the crystal packing is ensured by a complex hydrogen-bonds network that involves crystallization water molecules as well as π-stacking interactions. Indeed, phenyl groups of the free and coordinated ligands stack parallel to the *a*-axis. Free $(mip)^{2-}$ ligands are disordered. The disorder model is drawn in Scheme 2. Intramolecular chain Ce−Ce shortest distances are 10.2 Å. Shortest distances between Ce^{3+} ions that belong to neighboring chains are 10.8 Å along the *a*-axis and 6.0 and 6.9 Å in the *bc*-plane.

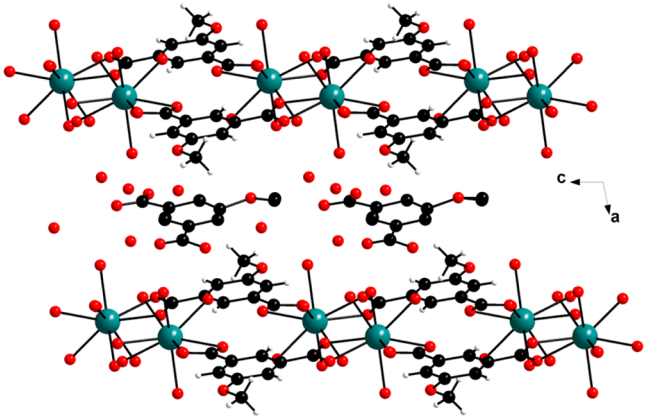

Figure 4. Projection view along the *b*-axis of $[Ce(mip)_{3/2}(H_2O)_5{\cdot}2H_2O]_\infty$.

Scheme 2. Schematic Representation of the Uncoordinated $(mip)^{2-}$ Ligand[a]

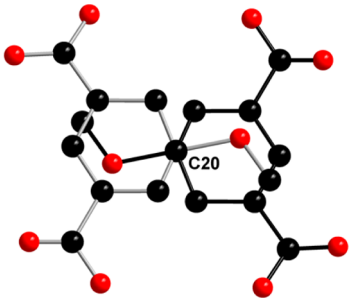

[a]The two equiprobable configurations of the free ligand, the one with light grey bonds and the one with black bonds, share the C20 atom.

$[Ln(mip)\ (Hmip)(H_2O)_5{\cdot}H_2O]_\infty$ with Ln = La, Ce, Pr, or Gd. Compounds that belong to the second series have general chemical formula $[Ln(mip)\ (Hmip)(H_2O)_5{\cdot}H_2O]_\infty$, where Ln symbolizes a lanthanide ion. These compounds have been obtained in gels as single crystals for Ln = La, Pr, and Gd, but they have only been obtained as microcrystalline powders for Ln = La or Ce. Crystal structure has been solved on the Gd-containing compound, and isostructurality of the La, Ce, and Pr derivatives has been assumed on the basis of X-ray diffraction measurements (Figure S4). This crystal structure can be described as the juxtaposition of 1D ribbon-like molecular motifs that spread parallel to the *b*-axis (Figure 5). There is only one crystallographically independent Gd^{3+} ion that is nine coordinated by four oxygen atoms from carboxylate functions and five oxygen atoms from coordination water molecules that form a slightly distorted capped square antiprism (Table S3).[52] Coordination modes of the $(mip)^{2-}$ ligand that links the Gd^{3+} ions are drawn in Figure 5.

In addition, there is one crystallization water molecule and one half-protonated ligand that lay between the ribbon-like molecular motifs (Scheme 3). The presence of an uncoordinated ligand between molecular motifs, which ensures the electroneutrality of the crystal structure, has already been observed in lanthanide-based coordination polymers obtained with 5-hydroxybenzene-1,3-dicarboxylate.[30] A complex network of hydrogen bonds and π-stacking interactions ensure the stability of the crystal structure.

Coupled thermal (ATG/DSC) and IR analyses have been performed (Figure S6). They show the departure of the six

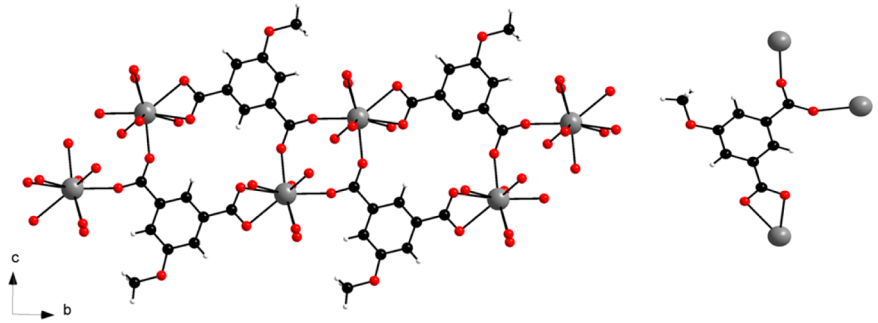

Figure 5. Left: Projection view along the *a*-axis of a ribbon-like molecular motif of $[Gd(mip)\ (Hmip)(H_2O)_5{\cdot}H_2O]_\infty$. Right: Coordination modes of the ligand $(mip)^{2-}$.

DOI: 10.1021/acs.cgd.6b01607
Cryst. Growth Des. 2017, 17, 1224−1234

Scheme 3. Perspective View of the Half-Protonated Ligand (Ball-and-Stick Model) between Two Ribbon-like Molecular Motifs in $[Gd(mip)(H(mip)(H_2O)_5{\cdot}H_2O]_\infty$[a]

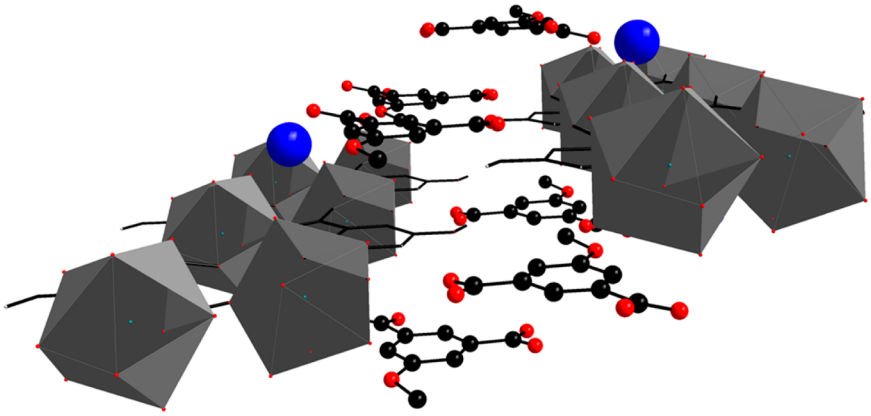

[a]Blue balls symbolize crystallization water molecules. Lanthanide ions coordination polyhedrons have been drawn, and hydrogen atoms have been omitted for clarity.

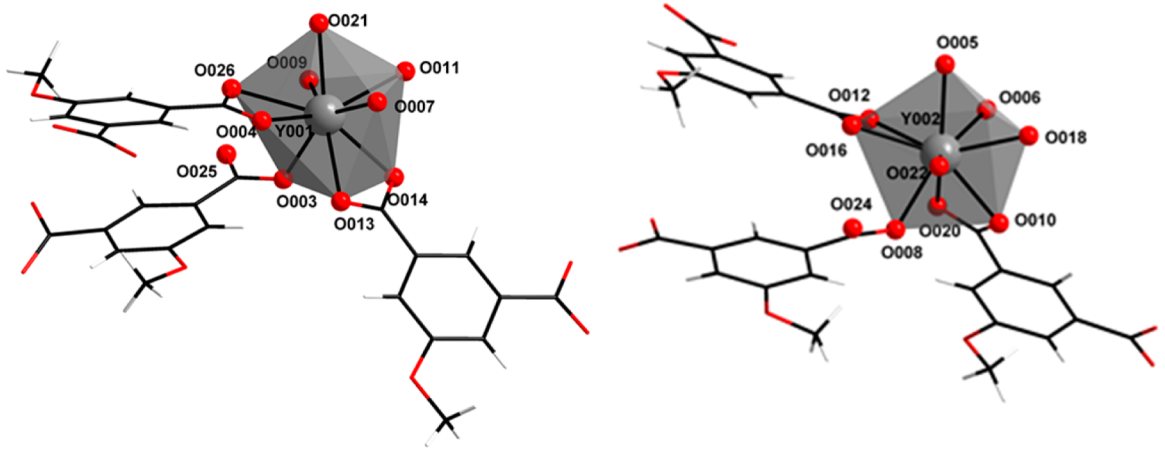

Figure 6. Extended coordination polyhedrons of Y1 (left) and Y2 (right) in $[Y_2(mip)_3(H_2O)_8{\cdot}4H_2O]_\infty$.

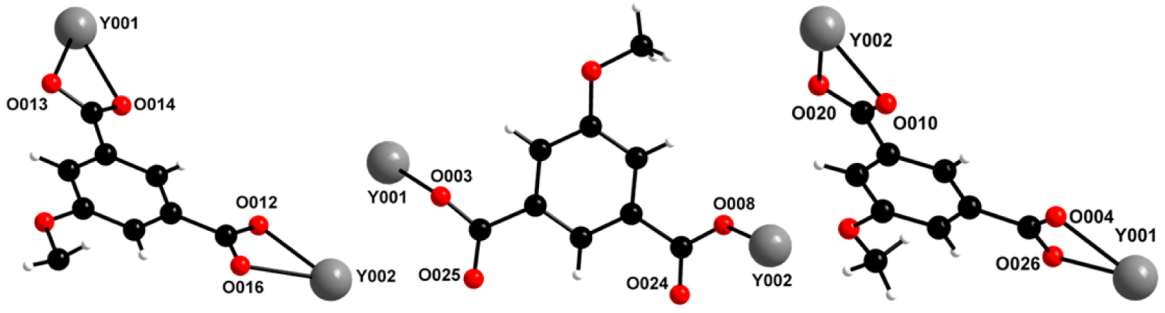

Figure 7. Coordination modes of the three independent ligands in $[Y_2(mip)_3(H_2O)_8{\cdot}4H_2O]_\infty$.

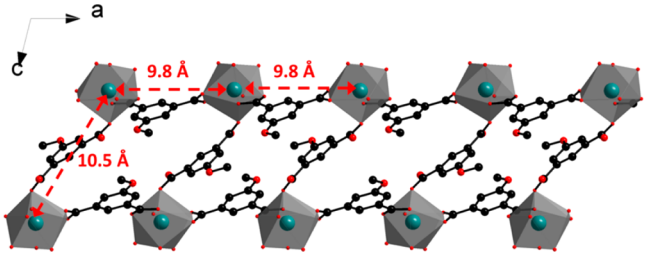

Figure 8. Ladder-like molecular motif in $[Y_2(mip)_3(H_2O)_8{\cdot}4H_2O]_\infty$. Hydrogen atoms have been omitted for clarity.

water molecules per lanthanide ion at about 100 °C (exptl, 20%; calcd, 17.3%).

It can be noticed that this crystal structure differs from the crystal structures of the lanthanide-based coordination polymers obtained with isophthalate, 5-aminoisophthalate or 5-hydroxyisophthalate.[28,30−32]

$[Ln_2(mip)_3(H_2O)_8{\cdot}4H_2O]_\infty$ with Ln = Sm−Tm plus Y. Compounds that have been obtained with lanthanide ions comprised between samarium and ytterbium plus yttrium constitute a family of isostructural compounds. Isostructurality of the compounds has been assumed on the basis of their powder X-ray diffraction patterns (Figure S5). The crystal

DOI: 10.1021/acs.cgd.6b01607
Cryst. Growth Des. 2017, 17, 1224−1234

Scheme 4. Schematic Projections Views of the Crystal Packing of $[Y_2(mip)_3(H_2O)_8{\cdot}4H_2O]_\infty$

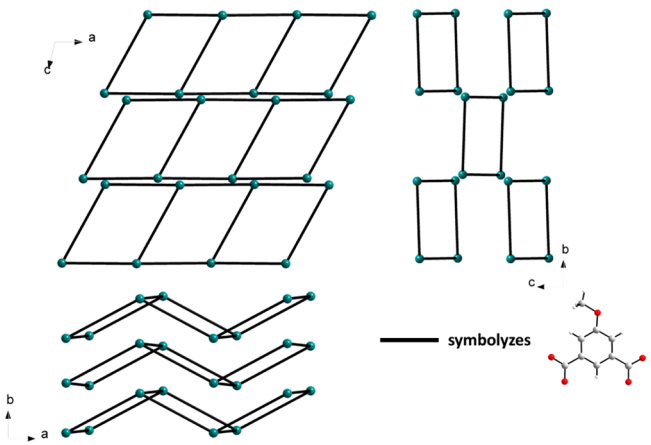

structure has been solved on the basis of a Y-containing single crystal. Once again this monodimensional crystal structure is completely different from those that had been obtained with isophthalate, 5-aminoisophthalate, or 5-hydroxyisophthalate.[28,30−32] There are two independent Y^{3+} ions in this crystal structure. Y1 and Y2 are both nine coordinated by five oxygen atoms from three carboxylate functions and four coordination water molecules that form slightly distorted capped square antiprisms[52] (Figure 6 and Table S4). Two out of the three independent ligands bind Y1 and Y2 in a bis-bidentate manner while the third one binds them in a bis-monodentate way (Figure 7).

The crystal structure can be described as the juxtaposition of wrapped ladder-like molecular motifs that spread parallel to the *a*-axis. Uprights are constituted by an alternation of Y^{3+} ions linked together by bis-bidentate ligands. Bis-monodentate ligands constitute the rungs of the ladder (Figure 8). Intermetallic distances between adjacent lanthanide ions that belong to the same molecular motif are close to 10 Å. These quite long intermetallic distances are rather rare in lanthanide-based coordination polymers made of polycarboxylates as ligands because carboxylate functions adopt commonly a bridging bis-monodentate coordination mode that leads to short Ln−Ln distances (~4.5 Å).[24] However, ladder-like molecular motifs stack in such a way that the shortest intermetallic contacts between lanthanide ions that belong to neighboring motifs are only 6 Å (see Scheme 4).

With the rough model that has been described previously,[53] the mean volume occupied by an Y^{3+} ion in this crystal structure is $\overline{v}$ = 464 Å^3; that is, the mean distance between two lanthanide ions is about 9.6 Å ($r = \sqrt[3]{\frac{3\overline{v}}{4\pi}}$). This is quite interesting as far as luminescence properties are targeted. Indeed, it is well-known[54] that intermetallic energy transfers are less efficient when the lanthanide ions are more than 10 Å far from each other. Therefore, in this crystal structure these energy transfers are expected to be weak.

Stability of the crystal packing is ensured by a strong hydrogen-bonds network that involves coordination and crystallization water molecules as well as oxygen atoms that belong to the ligands (see Table S5).

Coupled thermal analyses that have been performed on the basis of the Y-containing compound indicate a first weight loss centered at 125 °C that corresponds to the departure of the 12 water molecules per formula unit (exptl, 21.9%; calcd, 22.6%). The dehydrated phase that is obtained remains stable up to about 500 °C. At last the ligand decomposes and Y_2O_3 is obtained (See Figure S7). Thermodependent powder X-ray diffraction shows that the dehydrated phase observed between 100 and 500 °C is different from the initial hydrated one (Figure S8). Moreover, even when exposed to wet atmosphere, this phase does not rehydrate (Figure S9). The irreversibility of the structural change and the robustness of the dehydrated

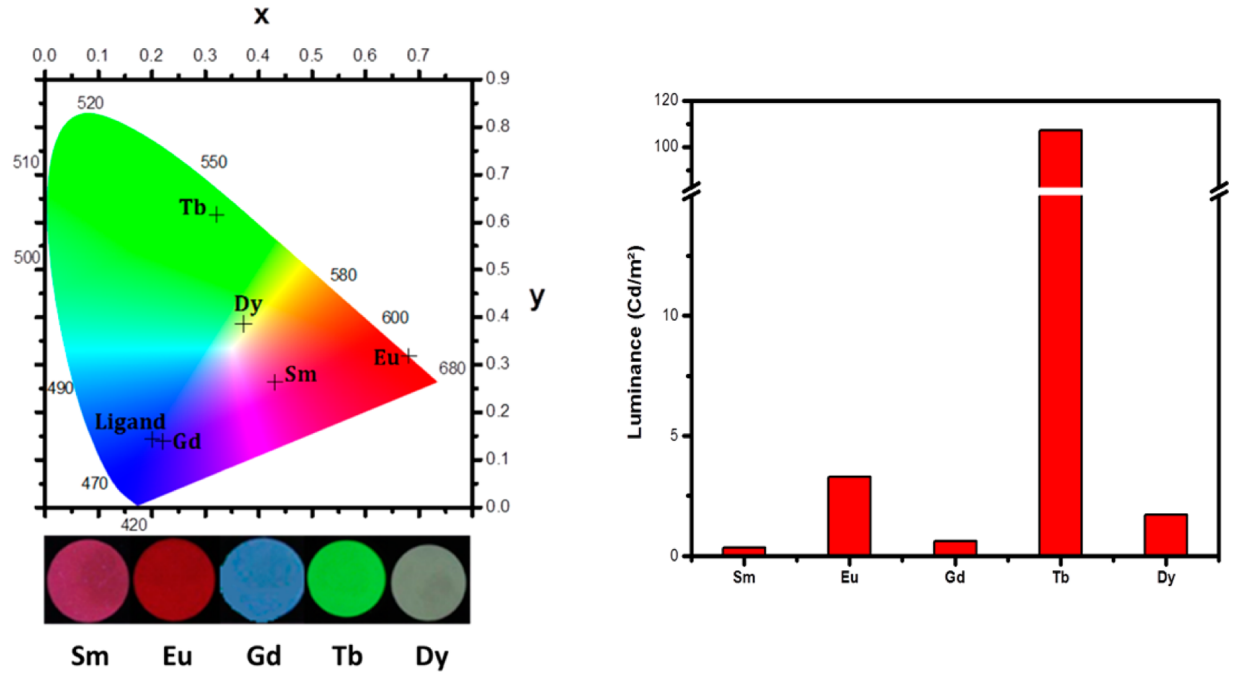

Figure 9. Left: Colorimetric coordinates and pictures under UV irradiation of $[Ln_2(mip)_3(H_2O)_8{\cdot}4H_2O]_\infty$ with Ln = Sm−Dy (λ_{exc} = 312 nm). Right: Luminance of $[Ln_2(mip)_3(H_2O)_8{\cdot}4H_2O]_\infty$ with Ln = Sm−Dy under UV excitation (λ_{exc} = 312 nm).

DOI: 10.1021/acs.cgd.6b01607
Cryst. Growth Des. 2017, 17, 1224−1234

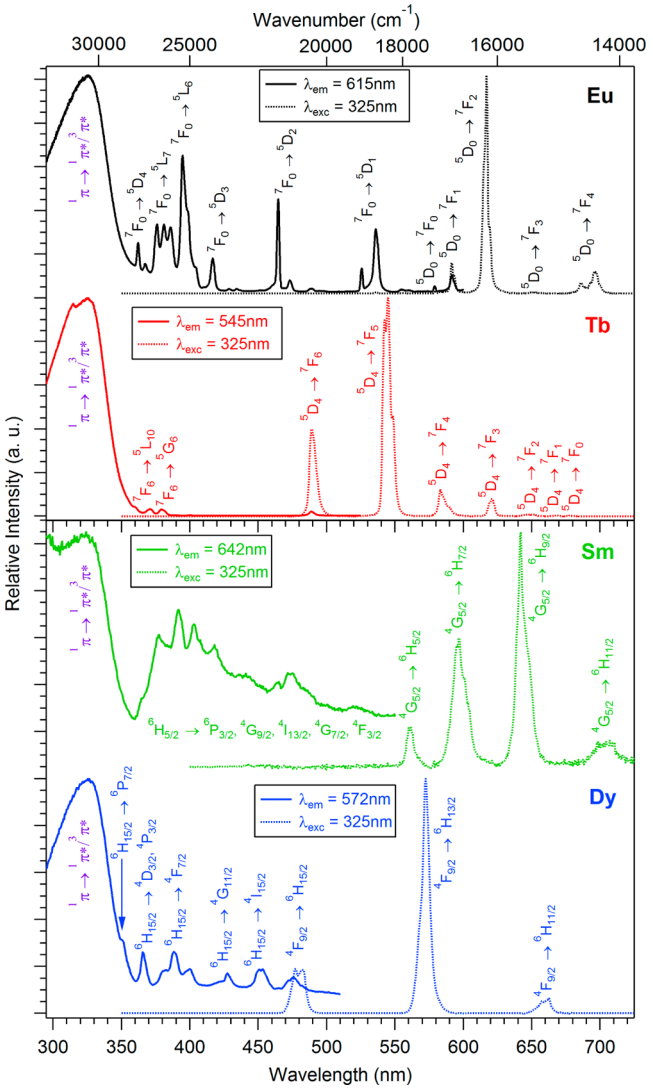

Figure 10. Excitation and emission spectra of $[Ln_2(mip)_3(H_2O)_8{\cdot}4H_2O]_\infty$ with Ln = Eu (black curves), Tb (red curves), Sm (green curves), and Dy (blue curves). λ_{exc} = 325 nm.

Table 4. Overall Quantum Yields and Luminescence Lifetimes of $[Ln_2(mip)_3(H_2O)_8{\cdot}4H_2O]_\infty$ with Ln = Sm, Eu, Tb, or Dy (λ_{exc} = 325 nm)

	Q_{Ln}^{ligand} (%)	τ_{obs}
$[Sm_2(mip)_3(H_2O)_8{\cdot}4H_2O]_\infty$	0.18(5)	<10 μs
$[Eu_2(mip)_3(H_2O)_8{\cdot}4H_2O]_\infty$	2.8(2)	0.21(1) ms
$[Tb_2(mip)_3(H_2O)_8{\cdot}4H_2O]_\infty$	41(3)	0.71(1) ms
$[Dy_2(mip)_3(H_2O)_8{\cdot}4H_2O]_\infty$	0.68(8)	<10 μs

phase could be related to the departure of four coordination water molecules per lanthanide ion and the presence of a noncoordinated oxygen atom from a carboxylate function in the vicinity of the undercrowded lanthanide ion that is available for coordination.

This series of compounds is of particular interest as far as strongly luminescent compounds are targeted. Indeed, the quite long mean intermetallic distance is supposed to favor luminescence because negligible intermetallic energy transfer is expected. Colorimetric coordinates and luminance of $[Ln_2(mip)_3(H_2O)_8{\cdot}4H_2O]_\infty$ with Ln = Sm–Dy are reported in Figure 9 and Table S6.

These measurements indicate that the luminance of the Tb-containing compound is significant (107 cd m^{-2}). Actually, to the best of our knowledge, among all the lanthanide-containing coordination polymers with benzene–polycarboxylate derivatives as ligands whose luminance has been measured to date, only $[Tb_2(bdc)_3{\cdot}4H_2O]_\infty$ (where bdc^{2-} stands for terephthalate) exhibits a higher luminance (142 cd m^{-2} under similar operating conditions).[49]

Excitation and emission spectra of the compounds that involve Sm^{3+}, Eu^{3+}, Tb^{3+}, or Dy^{3+} have been recorded (see Figure 10), and their calculated luminescence lifetimes and overall quantum yields are given in Table 4.

These measurements indicate that the antenna effect is effective for all compounds. Indeed the four compounds can be excited at the same wavelength that corresponds to ligand absorption. This was expected because the energy of the first excited singlet state of the ligand (29000 cm^{-1} estimated on the basis of the excitation spectrum (Figure S10) of $[Gd_2(mip)_3(H_2O)_8{\cdot}4H_2O]_\infty$) and of its first excited triplet state (24400 cm^{-1} estimated on the basis of the emission spectrum (Figure S10) recorded at 77 K of $[Gd_2(mip)_3(H_2O)_8{\cdot}4H_2O]_\infty$[55]) are supposed, according to Latva et al.'s[56] and Reinhouldt et al.'s[57] empirical rules, to favor efficient antenna effect ($\Delta E(^1\pi\pi^* - {}^3\pi\pi^*)$ = 4600 cm^{-1} < 5000 cm^{-1}). Additionally, it can be noticed that the phosphorescent lifetime of the triplet state is much longer (τ_{obs} = 39(3) ms) than the one measured for other coordination polymers (τ_{obs} = 7.0(1) ms for $[Gd_2(bdc)_3{\cdot}4H_2O]_\infty$).[49]

From a global point of view, it can be noticed that the overall quantum yields of the Eu-based compounds is very low compared with the one of the Tb-based compound (a factor 15 approximately). Because CH_3–O- is a + M and –I group, a photoinduced electron transfer (PET) may occur for the Eu-based compound as observed for 5-hydroxyisophthalate and 5-aminoisophtahlates derivatives.[28,30,31] On the other hand, intrinsic quantum yield is low (Q_{Eu}^{Eu} = 9.0(2)% measured with λ_{exc} = 464.5 nm that corresponds to the $^7F_0 \rightarrow {}^5D_2$ transition) which induces a low overall quantum yield despite sizable sensitization (η_{sens} = 30%[54]).

Unfortunately, it has not been possible to evaluate accurately the intrinsic quantum yield of the terbium derivative because the direct excitation transition ($^7F_6 \rightarrow {}^5G_6$) overlaps with the excitation band of the ligand. Furthermore, an excitation of the following $^7F_6 \rightarrow {}^5D_4$ transition at 489 nm does not allow accurate calculation of the intrinsic quantum yield of the Tb^{3+} ion because of a weak absorption. However, tentative measurements that have been performed seem to indicate that the sensitization of the Tb^{3+} ion by the ligand is very high and likely close to 100%.

For Sm- and Dy-based compounds, the overall quantum yields are lower than 1% indicating a weak antenna effect compared to Tb-based compounds (a factor 230 and 60 approximately with Sm and Dy, respectively).This can be attributed to the small energy gap between the emitting levels and the receiving levels of these two lanthanide ions.[54]

In recent years we have undertaken the investigation of heteronuclear lanthanide-based coordination polymers of formula $[Ln_{2-2x}Ln'_{2x}(L)_3(H_2O)_y]_\infty$ (with L = benzene–polycarboxylate ligand) in order to afford materials where both brightness and color can be modulated.[14,16,30,49] Such modification of the emissive properties when compared with homonuclear-based compounds is possible if strong intermetallic energy transfers are observed. In fact, for a given emissive

DOI: 10.1021/acs.cgd.6b01607
Cryst. Growth Des. 2017, 17, 1224–1234

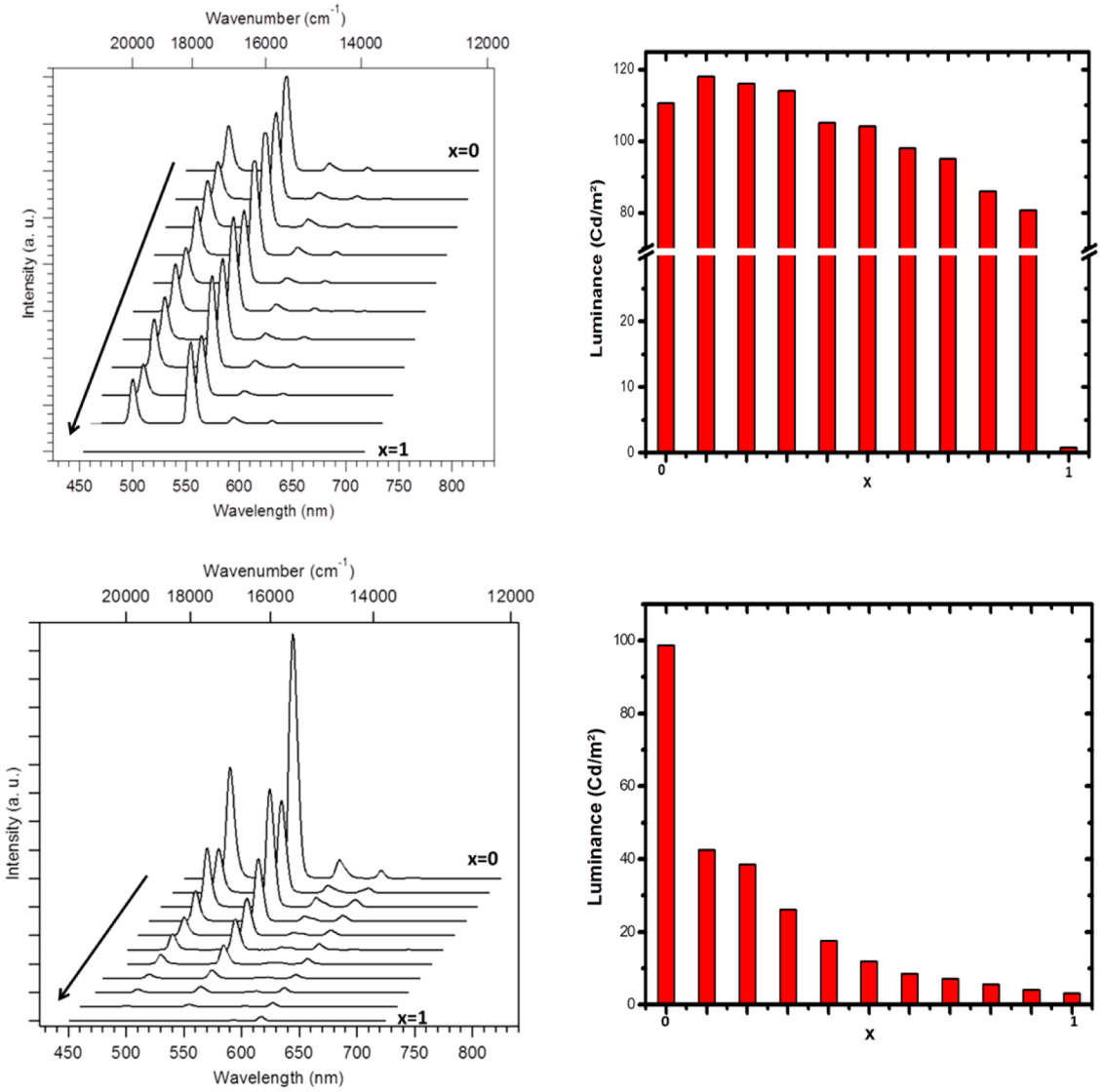

Figure 11. Emission spectra (left) and luminance measurements (right) under UV radiation (λ_{exc} = 325 nm) of $[Tb_{2-2x}Gd_{2x}(mip)_3(H_2O)_8{\cdot}4H_2O]_\infty$ with $0 \le x \le 1$ (top) and $[Tb_{2-2x}Eu_{2x}(mip)_3(H_2O)_8{\cdot}4H_2O]_\infty$ with $0 \le x \le 1$ (bottom).

compound, dilution with an optically inactive lanthanide ion (Gd^{3+} and so on) can enhance the brightness up to 20%,[49] whereas dilution with optically active ones leads to a color change. This last modification is however rather tricky to control as the obtained color depends on the relative position of the emissive energy levels as well as the intrinsic quantum yield of each lanthanide. As a result, one lanthanide can overwhelm the emission of the other as observed on $[Tb_{2-2x}Eu_{2x}(bdc)_3(H_2O)_4]_\infty$, where full red emission is visible for x as low as 0.2.[49]

The high Ln^{3+}−Ln^{3+} mean distance in family 2, makes it a nice platform to test the color modulation procedure with more predictable emission, ideally "additive color synthesis" as performed with classic dyes.

We have investigated two series of heterolanthanide coordination polymers with respective chemical formulas $[Tb_{2-2x}Gd_{2x}(mip)_3(H_2O)_8\cdot 4H_2O]_\infty$ and $[Tb_{2-2x}Eu_{2x}(mip)_3(H_2O)_8{\cdot}4H_2O]_\infty$ with $0 \le x \le 1$. The first series aims to quantify the intermetallic energy transfers and the second one to investigate the color modulation ability (Figure 11). All these compounds present the same crystal structure as those of the homolanthanide compounds (Figures S11 and S12). Accurate metallic composition of each compound has been measured by EDS measurements (Tables S7 and S8). Powder X-ray diffraction patterns show neither evidence of segregation of the lanthanide ions nor biphasic character of the microcrystalline powders.[49]

As anticipated, data that concern $[Tb_{2-2x}Gd_{2x}(mip)_3(H_2O)_8{\cdot}4H_2O]_\infty$ clearly show that there is little influence of the dilution of the Tb^{3+} ions by optically inactive Gd^{3+} ions. Indeed, luminance increases by only 7% for x = 0.1 which corresponds to a mean terbium-to-terbium distance of 10.7 Å. Then, it decreases progressively with the terbium content. This is clear evidence of the weak Tb−Tb intermetallic transfer within the series. In order to quantify this observation, we have calculated the intermetallic energy transfer rate (η_{ET} = 31(3)%) using the relationship $\eta_{ET} = 1 - \frac{\tau_{obs}}{\tau_0}$ (where τ_{obs} and τ_0 are the luminescent lifetimes in the presence or in the absence of an acceptor, respectively[54]) on the basis of the compounds $[TbEu(mip)_3(H_2O)_8{\cdot}4H_2O]_\infty$ (τ_{obs} = 0.45(3) ms) and $[TbGd(mip)_3(H_2O)_8{\cdot}4H_2O]_\infty$ (τ_0 = 0.72(2) ms). As a matter of comparison τ_{ET} was 95% for $[TbEu(bdc)_3(H_2O)_4]_\infty$.[49]

DOI: 10.1021/acs.cgd.6b01607
Cryst. Growth Des. 2017, 17, 1224−1234

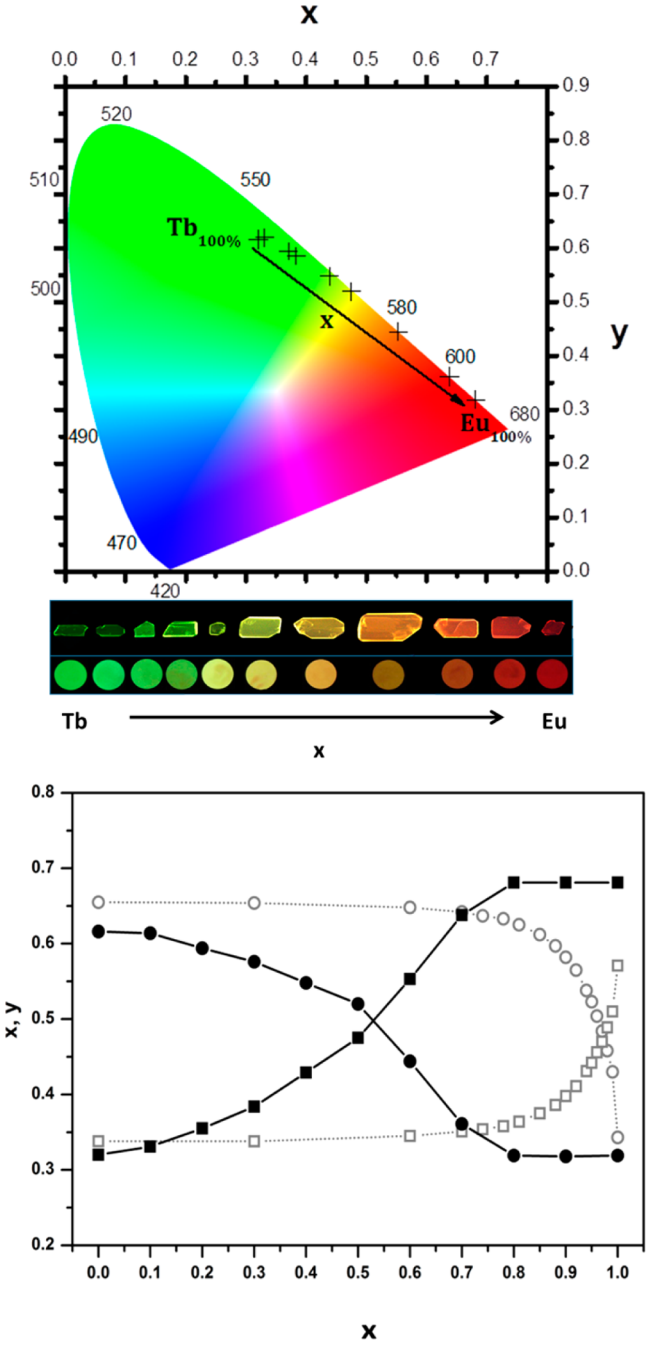

Figure 12. Colorimetric coordinates (top) and pictures of pellets of microcrystalline powders and of single crystals (middle) under UV irradiation (λ_{exc} = 312 nm) of $[Tb_{2-2x}Eu_{2x}(mip)_3(H_2O)_8{\cdot}4H_2O]_\infty$ with $0 \le x \le 1$. Bottom: comparison of the evolution of the colorimetric coordinates versus x of $[Tb_{2-2x}Eu_{2x}(mip)_3(H_2O)_8{\cdot}4H_2O]_\infty$ (low intermetallic energy transfer) in black and of $[Tb_{2-2x}Eu_{2x}(bdc)_3(H_2O)_4]_\infty$ (strong intermetallic transfer) in light gray. x and y colorimetric coordinates are symbolized by circles and squares, respectively. Curves that correspond to $[Tb_{2-2x}Eu_{2x}(bdc)_3(H_2O)_4]_\infty$ series are drawn from data in ref 49.

The second series, $[Tb_{2-2x}Eu_{2x}(mip)_3(H_2O)_8{\cdot}4H_2O]_\infty$, show a significant color change upon Eu addition but with a trend that is significantly different from the $[Tb_{2-2x}Eu_{2x}(bdc)_3(H_2O)_4]_\infty$ series (Figure 12).[24,49] As foreseen above, a regular variation from green to red is observed on the powders. This can be related to the weak Tb-to-Eu energy transfer. It is worth noticing that a similar trend is visible on single crystals that have been obtained by slow evaporation of the filtrates retrieved after the microcrystalline powders preparation. This further strongly suggests the monophasic character of the microcrystalline powders and the random distribution of the lanthanide ions over the metallic sites of the crystal structure.

CONCLUSION AND OUTLOOKS

In this work, we described the first three series of lanthanide-based coordination polymers with 5-methoxyisophthalate as ligand. One of the families is particularly interesting as far as potential applications are targeted. Indeed, the bright luminescence exhibited by some of the compounds that constitute this series associated with the weak intermetallic transfer allow new lanthanide ions combinations with new luminescent properties. In particular, the color modulation within a heteronuclear family is particularly efficient and predictable and can be based on a simple colors addition technique. This strategy could lead to molecular bar codes exhibiting luminescent properties in different spectral domains. We are convinced that this opens new opportunities in the field of anticounterfeiting taggants. Our group is currently working along this line.

ASSOCIATED CONTENT

Supporting Information

The Supporting Information is available free of charge on the ACS Publications Web site. The Supporting Information is available free of charge on the ACS Publications website at DOI: 10.1021/acs.cgd.6b01607.

Powder X-ray diffraction patterns of $Na_2(mip){\cdot}7H_2O$ (Figure S1), $[Ln(mip)(Hmip)(H_2O)_5{\cdot}H_2O]_\infty$ (Ln = La or Ce; Figure S4), $[Ln_2(mip)_3(H_2O)_8{\cdot}4H_2O]_\infty$ (Ln = Sm−Er plus Y; Figure S5), $[Y_2(mip)_3]_\infty$ (Figures S8 and S9), and $[Tb_{2-2x}Gd_{2x}(mip)_3(H_2O)_8{\cdot}4H_2O]_\infty$ ($0 \le x \le 1$; Figure S11) and $[Tb_{2-2x}Eu_{2x}(mip)_3(H_2O)_8{\cdot}4H_2O]_\infty$ ($0 \le x \le 1$; Figure S12), ATG/DSC of $Na_2(mip){\cdot}7H_2O$ (Figure S2), $[La(mip)(Hmip)(H_2O)_5].H_2O]_\infty$ (Figure S6), and $[Y_2(mip)_3(H_2O)_8{\cdot}4H_2O]_\infty$ (Figure S7) with additional IR spectral characterizations, UV−visible absorption spectrum of $Na_2(mip){\cdot}7H_2O$ (Figure S3), compound chemical analyses of families **1** and **2** (Table S1), continuous shape measurements of $[Ce(mip)_{3/2}(H_2O)_5{\cdot}2H_2O]_\infty$ (Table S2), $[Gd(mip)(Hmip)(H_2O)_5{\cdot}H_2O]_\infty$ (Table S3), and $[Ln_2(mip)_3(H_2O)_8{\cdot}4H_2O]_\infty$ (Table S4), selected hydrogen-bond distances in $[Y_2(mip)_3(H_2O)_8{\cdot}4H_2O]_\infty$ (Table S5), colorimetric coordinates and luminance of $Na_2(mip){\cdot}7H_2O$ and $[Ln_2(mip)_3(H_2O)_8{\cdot}4H_2O]_\infty$ with Ln = Sm−Dy (Table S6), UV−vis absorption spectrum of $[Gd_2(mip)_3(H_2O)_8{\cdot}4H_2O]_\infty$, excitation and emission spectra of $[Gd_2(mip)_3(H_2O)_8{\cdot}4H_2O]_\infty$ (Figure S10), and metallic contents for $[Tb_{2-2x}Gd_{2x}(mip)_3(H_2O)_8{\cdot}4H_2O]_\infty$ ($0 < x < 1$; Table S7) and $[Tb_{2-2x}Eu_{2x}(mip)_3(H_2O)_8{\cdot}4H_2O]_\infty$ ($0 < x < 1$; Table S8) (PDF)

Accession Codes

CCDC 1501130, 1501131, 1501139, and 1505544 contain the supplementary crystallographic data for this paper. These data can be obtained free of charge via www.ccdc.cam.ac.uk/data_request/cif, or by emailing data_request@ccdc.cam.ac.

DOI: 10.1021/acs.cgd.6b01607
Cryst. Growth Des. 2017, 17, 1224−1234

uk, or by contacting The Cambridge Crystallographic Data Centre, 12, Union Road, Cambridge CB2 1EZ, UK; fax: +44 1223 336033.

AUTHOR INFORMATION

Corresponding Authors

*(O.G.) E-mail: olivier.guillou@insa-rennes.fr.
*(C.D.) E-mail: carole.daiguebonne@insa-rennes.fr.

ORCID

Guillaume Calvez: 0000-0002-2133-7214
Olivier Guillou: 0000-0001-5946-8503

Notes

The authors declare no competing financial interest.

ACKNOWLEDGMENTS

The French Cooperation Agency in Senegal is acknowledged for financial support. The CDIFX of Rennes is acknowledged for single-crystal X-ray diffraction data collection.

REFERENCES

(1) Guillerm, V.; Weselinski, L.; Belmabkhout, Y.; Cairns, A. J.; D'Elia, V.; Wojtas, L.; Adil, K.; Eddaoudi, M. *Nat. Chem.* **2014**, *6*, 673−680.
(2) Eddaoudi, M.; Kim, J.; Rosi, N.; Vodak, D.; Wachter, J.; O'Keeffe, M.; Yaghi, O. M. *Science* **2002**, *295*, 469−472.
(3) Yaghi, O. M.; Li, G.; Li, H. *Nature* **1995**, *378*, 703−706.
(4) Yaghi, O. M.; Li, H. L. *J. Am. Chem. Soc.* **1995**, *117*, 10401−10402.
(5) Surblé, S.; Serre, C.; Millange, F.; Férey, G. *Solid State Sci.* **2006**, *8*, 413−417.
(6) Millange, F.; Serre, C.; Marrot, J.; Gardant, N.; Pelle, F.; Férey, G. *J. Mater. Chem.* **2004**, *14*, 642−645.
(7) Serre, C.; Millange, F.; Thouvenot, C.; Gardant, N.; Pelle, F.; Ferey, G. *J. Mater. Chem.* **2004**, *14*, 1540−1543.
(8) Kustaryono, D.; Kerbellec, N.; Calvez, G.; Freslon, S.; Daiguebonne, C.; Guillou, O. *Cryst. Growth Des.* **2010**, *10*, 775−781.
(9) Kerbellec, N.; Daiguebonne, C.; Bernot, K.; Guillou, O.; Le Guillou, X. *J. Alloys Compd.* **2008**, *451*, 377−383.
(10) Calvez, G.; Bernot, K.; Guillou, O.; Daiguebonne, C.; Caneschi, A.; Mahé, N. *Inorg. Chim. Acta* **2008**, *361*, 3997−4003.
(11) Jeon, J. R.; Clérac, R. *Dalton Trans.* **2012**, *41*, 9569−9586.
(12) Bernot, K.; Luzon, J.; Caneschi, A.; Gatteschi, D.; Sessoli, R.; Bogani, L.; Vindigni, A.; Rettori, A.; Pini, M. G. *Phys. Rev. B: Condens. Matter Mater. Phys.* **2009**, *79*, 134419.
(13) Yi, X.; Calvez, G.; Daiguebonne, C.; Guillou, O.; Bernot, K. *Inorg. Chem.* **2015**, *54*, 5213−5219.
(14) Fan, X.; Freslon, S.; Daiguebonne, C.; Le Polles, L.; Calvez, G.; Bernot, K.; Yi, X.; Huang, G.; Guillou, O. *Inorg. Chem.* **2015**, *54*, 5534−5546.
(15) Le Natur, F.; Calvez, G.; Daiguebonne, C.; Guillou, O.; Bernot, K.; Ledoux, J.; Le Polles, L.; Roiland, C. *Inorg. Chem.* **2013**, *52*, 6720−6730.
(16) Freslon, S.; Luo, Y.; Daiguebonne, C.; Calvez, G.; Bernot, K.; Guillou, O. *Inorg. Chem.* **2016**, *55*, 794−802.
(17) Lan, A. J.; Li, K. H.; Wu, H. H.; Olson, D. H.; Emge, T. J.; Ki, W.; Hong, M. C.; Li, J. *Angew. Chem., Int. Ed.* **2009**, *48*, 2334−2338.
(18) Feng, J.; Zhang, H. J. *Chem. Soc. Rev.* **2013**, *42*, 387−410.
(19) Cui, Y.; Yue, Y.; Qian, G.; Chen, B. *Chem. Rev.* **2012**, *112*, 1126−1162.
(20) Cui, Y.; Xu, H.; Yue, Y.; Guo, Z.; Yu, J.; Chen, Z.; Gao, J.; Yang, Y.; Qian, G.; Chen, B. *J. Am. Chem. Soc.* **2012**, *134*, 3979−3982.
(21) Serre, C.; Millange, F.; Thouvenot, C.; Gardant, N.; Pelle, F.; Ferey, G. *J. Mater. Chem.* **2004**, *14*, 1540−1543.
(22) Reddy, M. L. P.; Sivakumar, S. *Dalton Trans.* **2013**, *42*, 2663−2678.
(23) Guillou, O.; Daiguebonne, C.; Calvez, G.; Bernot, K. *Acc. Chem. Res.* **2016**, *49*, 844−856.
(24) Kerbellec, N.; Kustaryono, D.; Haquin, V.; Etienne, M.; Daiguebonne, C.; Guillou, O. *Inorg. Chem.* **2009**, *48*, 2837−2843.
(25) Yang, Q. Y.; Pan, M.; Wei, S. C.; Li, K.; Du, B. B.; Su, C. Y. *Inorg. Chem.* **2015**, *54*, 5707−5716.
(26) Daiguebonne, C.; Gérault, Y.; Guillou, O.; Lecerf, A.; Boubekeur, K.; Batail, P.; Kahn, M.; Kahn, O. *J. Alloys Compd.* **1998**, *275−277*, 50−53.
(27) Guillou, O.; Daiguebonne, C. Lanthanide-containing coordination polymers. In *Handbook on the Physics and Chemistry of Rare Eaths*, Vol. *34*; Gschneider, K. A., Jr., Bünzli, J. C. G., Pecharsky, V. K., Eds.; Elsevier: Amsterdam, 2004; pp 359−404, DOI: 10.1016/S0168-1273(04)34004-3.
(28) Freslon, S.; Luo, Y.; Calvez, G.; Daiguebonne, C.; Guillou, O.; Bernot, K.; Michel, V.; Fan, X. *Inorg. Chem.* **2014**, *53*, 1217−1228.
(29) Fan, X.; Daiguebonne, C.; Guillou, O.; Camara, M. *Acta Crystallogr., Sect. E: Struct. Rep. Online* **2014**, *E70*, m181−m182.
(30) Fan, X.; Freslon, S.; Daiguebonne, C.; Calvez, G.; Le Polles, L.; Bernot, K.; Guillou, O. *J. Mater. Chem. C* **2014**, *2*, 5510−5525.
(31) Luo, Y.; Calvez, G.; Freslon, S.; Bernot, K.; Daiguebonne, C.; Guillou, O. *Eur. J. Inorg. Chem.* **2011**, *2011*, 3705−3716.
(32) Daiguebonne, C.; Kerbellec, N.; Gérault, Y.; Guillou, O. *J. Alloys Compd.* **2008**, *451*, 372−376.
(33) Mc Cormick, L. J.; Morris, S. A.; Teat, S. J.; Mc Pherson, M. J.; Slawin, A. M. Z.; Morris, R. E. *Dalton Trans.* **2015**, *44*, 17686−17695.
(34) Zhang, H.-J. *Z. Kristallogr. - New Cryst. Struct.* **2011**, *226*, 629−630.
(35) Tian, C.; Lin, Z.; Du, S. *Cryst. Growth Des.* **2013**, *13*, 3746−3753.
(36) Desreux, J. F. In *Lanthanide Probes in Life, Chemical and Earth Sciences*; Bünzli, J.-C. G., Choppin, G. R., Eds.; Elsevier: Amsterdam, 1989; p 43.
(37) Henisch, H. K. *Crystals in Gels and Liesegang Rings*; Cambridge University Press: Cambridge, U.K., 1988.
(38) Henisch, H. K.; Rustum, R. *Crystal Growth in Gels*; The Pennsylvania State University Press: University Park, PA, USA, 1970; pp 1−196.
(39) Daiguebonne, C.; Deluzet, A.; Camara, M.; Boubekeur, K.; Audebrand, N.; Gérault, Y.; Baux, C.; Guillou, O. *Cryst. Growth Des.* **2003**, *3*, 1015−1020.
(40) Sheldrick, G. M. *Acta Crystallogr., Sect. A: Found. Crystallogr.* **2008**, *64*, 112−122.
(41) *SAINT*, V837A; Brucker: Madison, WI, USA, 2014.
(42) *SADABS*, 2014/5; Bruker: Madison, WI, USA, 2014.
(43) *APEX3*; Bruker: Madison, WI, USA, 2015.
(44) Altomare, A.; Burla, M. C.; Camalli, M.; Carrozzini, B.; Cascarano, G.; Giacovazzo, C.; Guagliardi, A.; Moliterni, A. G. G.; Polidori, G.; Rizzi, A. C. *J. Appl. Crystallogr.* **1999**, *32*, 339−340.
(45) Sheldrick, G. M.; Schneider, T. R. *Methods Enzymol.* **1997**, *277*, 319−343.
(46) Farrugia, L. J. *J. Appl. Crystallogr.* **2012**, *45*, 849−854.
(47) Roisnel, T.; Rodriquez-Carvajal, J. *Mater. Sci. Forum* **2001**, *378-381*, 118−123.
(48) Kraus, W.; Nolze, G. *J. Appl. Crystallogr.* **1996**, *29*, 301−303.
(49) Haquin, V.; Etienne, M.; Daiguebonne, C.; Freslon, S.; Calvez, G.; Bernot, K.; Le Polles, L.; Ashbrook, S. E.; Mitchell, M. R.; Bünzli, J.-C.; Eliseeva, S. V.; Guillou, O. *Eur. J. Inorg. Chem.* **2013**, *2013*, 3464−3476.
(50) Wyszecki, G. Colorimetry. In *Handbook of Optics*; Driscoll, W. G., Vaughan, W., Eds.; McGraw-Hill: New York, 1978; pp 1−15.
(51) *Method of Measuring and Specifying Colour Rendering Properties of Light Sources*, CIE Technical Report 013-3; International Commission on Illumination (CIE): Vienna, Austria, 1995; p 16.
(52) Casanova, D.; Llunell, M.; Alemany, P.; Alvarez, S. *Chem. - Eur. J.* **2005**, *11*, 1479−1494.
(53) Luo, Y.; Zheng, Y.; Calvez, G.; Freslon, S.; Bernot, K.; Daiguebonne, C.; Roisnel, T.; Guillou, O. *CrystEngComm* **2013**, *15*, 706−720.

DOI: 10.1021/acs.cgd.6b01607
Cryst. Growth Des. 2017, 17, 1224−1234

(54) Bünzli, J.-C. G.; Eliseeva, S. V. Basics of lanthanide photophysics. In *Lanthanide Luminescence*; Hänninen, P., Härmä, H., Eds.; Springer: Berlin, Heidelberg, 2010; pp 1−45, DOI: 10.1007/4243_2010_3.
(55) Gutierrez, F.; Tedeschi, C.; Maron, L.; Daudey, J.-P.; Poteau, R.; Azema, J.; Tisnes, P.; Picard, C. *Dalton Trans.* **2004**, 1334−1347.
(56) Latva, M.; Takalo, H.; Mukkala, V.-M.; Matachescu, C.; Rodriguez-Ubis, J. C.; Kankare, J. *J. Lumin.* **1997**, *75*, 149−169.
(57) Steemers, F. J.; Verboom, W.; Reinhoudt, D. N.; Van der Tol, E. B.; Verhoeven, J. W. *J. Am. Chem. Soc.* **1995**, *117*, 9408−9414.

DOI: 10.1021/acs.cgd.6b01607
Cryst. Growth Des. 2017, 17, 1224−1234